J|A|C|S
ARTICLES
Published on Web 12/03/2004

Directly *meso*−*meso* Linked Porphyrin Rings: Synthesis, Characterization, and Efficient Excitation Energy Hopping

Yasuyuki Nakamura,[†] In−Wook Hwang,[‡] Naoki Aratani,[†] Tae Kyu Ahn,[‡] Dah Mee Ko,[‡] Akihiko Takagi,[§] Tomoji Kawai,[§] Takuya Matsumoto,[§] Dongho Kim,*[,‡] and Atsuhiro Osuka*[,†]

Department of Chemistry, Graduate School of Science, Kyoto University, and Core Research for Evolutional Science and Technology (CREST), Japan Science and Technology Agency (JST), Sakyo-ku, Kyoto 606-8502, Japan; Center for Ultrafast Optical Characteristics Control and Department of Chemistry, Yonsei University, Seoul 120-749, Korea; and the Institute of Scientific and Industrial Research (ISIR), Osaka University, Core Research for Evolutional Science and Technology (CREST), Japan Science and Technology Agency (JST), Mihogaoka, Ibaragi, Osaka 567-0047, Japan

Received August 6, 2004; E-mail: osuka@kuchem.kyoto-u.ac.jp; dongho@yonsei.ac.kr

Abstract: Directly *meso*−*meso* linked porphyrin rings **CZ4**, **CZ6**, and **CZ8** that respectively comprise four, six, and eight porphyrins have been synthesized in a stepwise manner from a 5,10-diaryl zinc(II) porphyrin building block. Symmetric cyclic structures have been indicated by their very simple ^{1}H NMR spectra that exhibit only a single set of porphyrin and their absorption spectra that display a characteristic broad nonsplit Soret band around 460 nm. Energy minimized structures calculated at the B3LYP/6-31G* level indicate that a dihedral angle between neighboring porphyrins decreases in order of **CZ6** > **CZ8** > **CZ4**, which is consistent with the ^{1}H NMR data. Photophysical properties of these molecules have been examined by the steady-state absorption, fluorescence, fluorescence lifetime, fluorescence anisotropy decay, and transient absorption measurements. Both the pump-power dependence on the femtosecond transient absorption and the transient absorption anisotropy decay profiles are directly related with the excitation energy migration processes within the porphyrin rings, where the exciton−exciton annihilation time and the polarization anisotropy rise time are well described in terms of the Förster-type incoherent energy hopping model. Consequently, the excitation energy hopping rates have been estimated for **CZ4** $(119 \pm 2 \text{ fs})^{-1}$, **CZ6** $(342 \pm 59 \text{ fs})^{-1}$, and **CZ8** $(236 \pm 31 \text{ fs})^{-1}$, which reflect the magnitude of the electronic coupling between the neighboring porphyrins. Overall, these porphyrin rings serve as a well-defined wheel-shaped light harvesting antenna model in light of very efficient excitation energy hopping along the ring.

Introduction

In the bacterial photosynthetic antenna of LH1 and LH2, photosynthetic tetrapyrrolic pigments are deliberately positioned in a wheel-like arrangement, hence manipulating the absorbed light energy through intrawheel efficient excitation energy hopping (EEH) processes.[1] Stimulated by these beautiful architectures, several cyclic and dendritic porphyrin arrays have been explored and intramolecular EEH processes therein have been studied.[2−9] Despite these extensive efforts, efficient EEH that rivals those in the natural photosynthetic antenna has hardly been achieved so far. It is expecetd that the regular cyclic

[†] Kyoto University.
[‡] Yonsei University.
[§] Osaka University.

(1) (a) McDermott, G.; Prince, S. M.; Freer, A. A.; Hawthornthwaite-Lawless, A. M.; Papiz, M. Z.; Cogdell, R. J.; Isaacs, N. W. *Nature* **1995**, *374*, 517. (b) Karrasch, S.; Bullough, P. A.; Ghosh, R. *EMBO J.* **1995**, *14*, 631. (c) Koepke, J.; Hu, X.; Muenke, C.; Schulten, K.; Michel, H. *Structure* **1996**, *4*, 581. (d) McLuskey, K.; Prince, S. M.; Cogdell, R. J.; Isaacs, N. W. *Biochemistry* **2001**, *40*, 8783. (e) Roszak, A. W.; Howard, T. D.; Southall, J.; Gardiner, A. T.; Law, C. J.; Isaacs, N. W.; Cogdell, R. J. *Science* **2003**, *302*, 1969.

(2) (a) Anderson, H. L.; Sanders, J. K. M. *J. Chem. Soc., Chem. Commun.* **1989**, 1714. (b) Anderson, H. L.; Sanders, J. K. M. *Angew. Chem., Int. Ed. Engl.* **1990**, *29*, 1400. (c) Anderson, S.; Anderson, H. L.; Sanders, J. K. M. *Acc. Chem. Res.* **1993**, *26*, 469. (d) Dubowchik, G.; Hamilton, A. D. *J. Chem. Soc., Chem. Commun.* **1987**, 293.

(3) (a) Wagner, R. W.; Seth, J.; Yang, S. I.; Kim, D.; Bocian, D. F.; Holten, D.; Lindsey, J. S. *J. Org. Chem.* **1998**, *63*, 5042. (b) Li, J.; Ambroise, A.; Yang, S. I.; Diers, J. R.; Seth, J.; Wack, C. R.; Bocian, D. F.; Holten, D.; Lindsey, J. S. *J. Am. Chem. Soc.* **1999**, *121*, 8927. (c) Ambroise, A.; Li, J.; Yu, L.; Lindsey, J. S. *Org. Lett.* **2000**, *2*, 2563.

(4) (a) Biemans, H. A. M.; Rowan, A. E.; Verhoeven, A.; Vanoppen, P.; Latterini, L.; Foekema, J.; Schenning, A. P. H. J.; Meijer, E. W.; de Schryver, F. C.; Nolte, R. J. M. *J. Am. Chem. Soc.* **1998**, *120*, 11054. (b) Schweitzer, G.; De Belder, G.; Latterini, L.; Karini, Y.; Rowan, A. E.; Nolte, R. J. M.; de Schryver F. C. *Chem. Phys. Lett.* **1999**, *303*, 261. (c) Lensen, M. C.; van Dingenen, S. J. T.; Elemans, J. A. A.; Dijkstra, H. P.; van Klinc, G. P. M.; van Koten, G.; Gerritsen, J. W.; Speller, S.; Nolte, R. J. M.; Rowan, A. E. *Chem. Commun.* **2004**, 762. (d) Lensen, M. C.; Takazawa, K.; Elemans, J. A. A. W.; Jeukens, C. R. L. P. N.; Christianen, P. C. M.; Maan, J. C.; Rowan, A. E.; Nolte, R. J. M. *Chem.*−*Eur. J.* **2004**, *10*, 831.

(5) (a) Sugiura, K.; Fujimoto, Y.; Sakata, Y. *Chem. Commun.* **2000**, 1105. (b) Kato, A.; Sugiura, K.; Miyasaka, H.; Tanaka, H.; Kawai, T.; Sugimoto, M.; Yamashita, M. *Chem. Lett.* **2004**, *33*, 578.

(6) (a) Mongin, O.; Papamicaël, C.; Hoyler, N.; Gossauer, A. *J. Org. Chem.* **1998**, *63*, 5568. (b) Mongin, O.; Schuwey, A.; Vallot, M.-A.; Gossauer, A. *Tetrahedron Lett.* **1999**, *40*, 8347. (c) Brodard, P.; Matzinger, S.; Vauthey, E.; Mongin, O.; Papamicaël, C.; Gossauer, A. *J. Phys. Chem. A* **1999**, *103*, 5858. (d) Mongin, O.; Hoyler, N.; Gossauer, A. *Eur. J. Org. Chem.* **2000**, 1193. (e) Rucareanu, S.; Mongin, O.; Schuwey, A.; Hoyler, N.; Gossauer, A. Amrein, W.; Hediger, H.-U. *J. Org. Chem.* **2001**, *66*, 4973.

 10.1021/ja045254p CCC: $30.25

Chart 1. Structures of **CZ4**, **CZ6**, and **CZ8** (Ar = 3,5-Di-*tert*-butylphenyl)

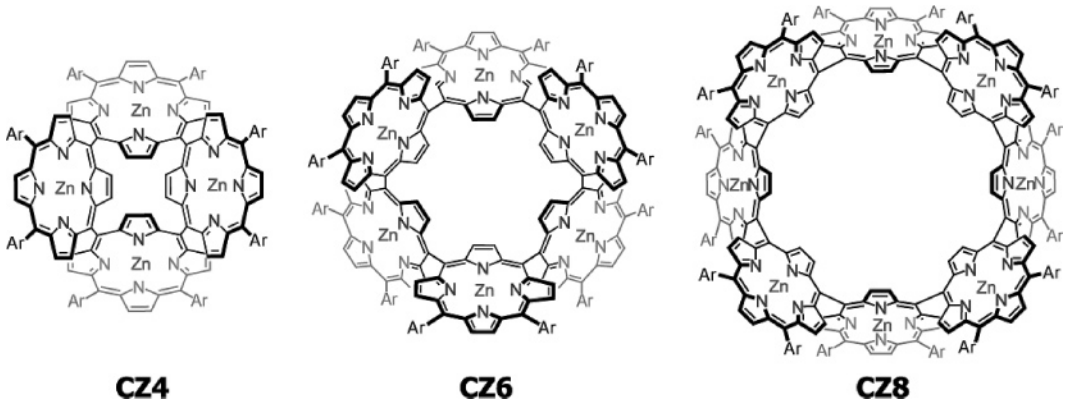

arrangement and the large electronic coupling between neighboring pigments are required for efficient EEH.

In the past decade, we have explored various directly *meso*−*meso* linked porphyrin arrays on the basis of silver(I)-promoted coupling of a 5,15-diaryl-substituted zinc porphyrin.[10,11] Some of these porphyrin arrays are promising as optical molecular wire by transmitting excitation energy over a long distance. Actually, the efficient excitation energy transfer has been achieved over a long distance through *meso*−*meso* linked zinc(II) porphyrin arrays.[11] This function relies on their strongly coupled but not fully π-conjugated electronic character.[12] Recently, we reported a dodecameric porphyrin wheel, in which *meso*−*meso* linked diporphyrin subunits are bridged by a 1,3-phenylene spacer that is used to produce curvature of array.[13] The presence of such a spacer weakens the electronic coupling and causes two different EEH steps with rates of 0.24 ps^{-1} and 3.6 ps^{-1}, which correspond to EEH within a *meso*−*meso* linked diporphyrin and between neighboring *meso*−*meso* linked diporphyrins.

Cyclic porphyrin architectures, in which the constituent porphyrins are all directly linked at *meso*−*meso* positions, are a more attractive target in view of synthetic challenge, higher molecular symmetry, and large and regular electronic interaction between neighboring porphyrins that will lead to efficient EEH. Such molecules can be regarded as a genuine *porphyrin ring* whose electronic π-network consists of only porphyrins and thus may be interesting also in view of belt-shape aromatic molecules that consist of only aromatic segments.[14] In addition, these molecules will allow direct comparison of molecular morphology effects, *linear* versus *cyclic*, upon the overall photophysical properties of *meso*−*meso* linked porphyrin arrays. In this paper, we report the syntheses and characterizations of porphyrin rings such as **CZ4**, **CZ6**, and **CZ8** (Chart 1) and their photophysical properties.

Experimental Section

General Information. The syntheses of **CZ4**, **CZ6**, and **CZ8** as well as the intermediates leading to them are detailed in the Supporting Information. All solvents were spectrophotometric grade. All the calculations were carried out using the Gaussian 03 program. All structures were optimized with Becke's three-parameter hybrid exchange functional and the Lee−Yang−Parr correlation functional (B3LYP), employing the 6-31G* basis set for all atoms.

STM Images. Clean flat Cu(100) surfaces were obtained by Ar^+ sputtering and annealing (550°C) cycles for a substrate. The porphyrin ring molecules dissolved into CH_2Cl_2 were deposited by spraying ca. 0.5 μL of the solution onto the substrate in a vacuum (10^{-6} mbar) using a pulse injection method,[15] which is suited for deposition of large fragile molecules with escaping decomposition often encountered in sample deposition from the gas phase. In situ STM measurements were performed at room temperature in an ultrahigh vacuum ($<10^{-10}$ mbar) with a home-build STM by using an electrochemical etched Pt/Ir tip. STM image was obtained in constant height mode.

Steady-State Spectra. The samples were prepared in micromolar concentrations in THF (spectroscopic grade). Absorption spectra were obtained with a Shimadzu model 1601 UV spectrometer, and steady-state fluorescence was measured by a Hitachi model F-4500 fluorescence spectrophotometer at room temperature.

(7) (a) Takase, M.; Ismael, R.; Murakami, R.; Ikeda, M.; Kim, D.; Shinmori, H.; Furuta, H.; Osuka, A. *Tetrahedron Lett.* **2002**, *43*, 5157. (b) Cho, H. S.; Rhee, H.; Song, J. K.; Min, C.-K.; Takase, M.; Aratani, N.; Cho, S.; Osuka, A.; Joo, T.; Kim, D. *J. Am. Chem. Soc.* **2003**, *125*, 5849.

(8) (a) Choi, M.-S.; Yamazaki, T.; Yamazaki, I.; Aida, T. *Angew. Chem., Int. Ed.* **2004**, *43*, 150. (b) Choi, M.-S.; Aida, T.; Yamazaki, T.; Yamazaki, I. *Chem.—Eur. J.* **2002**, *8*, 2668. (c) Choi, M.-S.; Aida, T.; Luo, H.; Araki, Y.; Ito, O. *Angew. Chem., Int. Ed.* **2003**, *42*, 4060. (d) Yeow, E. K. L.; Ghiggino, K. P.; Reek, J. N. H.; Crossley, M. J.; Bosman, A. W.; Schenning, A. P. H. J.; Meijer, E. W. *J. Phys. Chem. B* **2000**, *104*, 2596.

(9) Noncovalent porphyrin assemblies were reported. (a) Drain, C. M. Nifiatis, F.; Vasenko, A.; Batteas, J. D. *Angew. Chem., Int. Ed.* **1998**, *37*, 2344. (b) Rubtsov, I. V.; Kobuke, Y.; Miyaji, H.; Yoshihara, K. *Chem. Phys. Lett.* **1999**, *308*, 323. (c) Takahashi, R.; Kobuke, Y. *J. Am. Chem. Soc.* **2003**, *125*, 2372. (d) Ikeda, C.; Satake, A.; Kobuke, Y. *Org. Lett.* **2003**, *5*, 4935. (e) Kuramochi, Y.; Satake, A.; Kobuke, Y. *J. Am. Chem. Soc.* **2004**, *126*, 8668, and refs 3c and 6d.

(10) (a) Osuka, A.; Shimidzu, H. *Angew. Chem., Int. Ed. Engl.* **1997**, *36*, 135. (b) Aratani, N.; Osuka, A.; Kim, Y. H.; Jeong, D. H.; Kim, D. *Angew. Chem., Int. Ed.* **2000**, *39*, 1458.

(11) (a) Nakano, A.; Osuka, A.; Yamazaki, I.; Yamazaki, T.; Nishimura, Y. *Angew. Chem., Int. Ed.* **1998**, *37*, 3023. (b) Nakano, A.; Yamazaki, T.; Nishimura, Y.; Yamazaki, I.; Osuka, A. *Chem.—Eur. J.* **2000**, *6*, 3254. (c) Aratani, N.; Cho, H. S.; Ahn, T. K.; Cho, S.; Kim, D.; Sumi, H.; Osuka, A. *J. Am. Chem. Soc.* **2003**, *125*, 9668.

(12) (a) Kim, D.; Osuka, A. *J. Phys. Chem. A* **2003**, *107*, 8791. (b) Kim, Y. H.; Jeong, D. H.; Kim, D.; Jeoung, S. C.; Cho, H. S.; Kim, S. K.; Aratani, N.; Osuka, A. *J. Am. Chem. Soc.* **2001**, *123*, 76.

(13) Peng, X.; Aratani, N.; Takagi, A.; Matsumoto, T.; Kawai, T.; Hwang, I.-W.; Ahn, T. K.; Kim, D.; Osuka, A. *J. Am. Chem. Soc.* **2004**, *126*, 4468.

(14) (a) Ashton, P. R.; Isaacs, N. S.; Kohnke, F. H.; Slawin, A. M. Z.; Spencer, C. M.; Stoddart, J. F.; Williams, D. J. *Angew. Chem., Int. Ed. Engl.* **1988**, *27*, 966. (b) Diederich, F. *Nature* **1994**, *369*, 199. (c) Kawase, T.; Darabi, H. R.; Oda, M. *Angew. Chem., Int. Ed. Engl.* **1996**, *35*, 2664. (d) Hensel, V.; Schlüter, A. D. *Chem.—Eur. J.* **1999**, *5*, 421. (e) Krömer, J.; Rios-Carreras, I.; Fuhrmann, G.; Musch, C.; Wunderlin, M.; Debaerdemaeker, T.; Mena-Osteritz, E.; Bäuerle, R. *Angew. Chem., Int. Ed.* **2000**, *39*, 3481. (f) Ohkita, M.; Ando, K.; Tsuji, T. *Chem. Commun.* **2001**, 2570. (g) Fuhrmann, G.; Debaerdemaeker, T.; Bäuerle, P. *Chem. Commun.* **2003**, 948. (h) Seidel, D.; Lynch, V.; Sessler, J. L. *Angew. Chem., Int. Ed.* **2002**, *41*, 1422. (i) Köhler, T.; Seidel, D.; Lynch, V.; Arp. F. O.; Ou, Z.; Kadish, K. M.; Sessler, J. L. *J. Am. Chem. Soc.* **2003**, *125*, 6872. (j) Neudorff, W. D.; Lentz, D.; Anibarro, M.; Schlüter, A. D. *Chem.—Eur. J.* **2003**, *9*, 2745. (k) Kawase, T.; Tanaka, K.; Fujiwara, N.; Darabi, R. H.; Oda, M. *Angew. Chem., Int. Ed.* **2003**, *42*, 1624. (l) Matsuo, Y.; Tahara, K.; Sawamura, M.; Nakamura, E. *J. Am. Chem. Soc.* **2004**, *126*, 8725.

(15) (a) Tanaka, H.; Nakagawa, T.; Kawai, T. *Surf. Sci.* **1996**, *364*, L575. (b) Takagi, A.; Yanagawa, Y.; Tsuda, A.; Aratani, N.; Matsumoto, T.; Osuka, A.; Kawai, T. *Chem. Commun.* **2003**, 2986.

Time-Resolved Fluorescence. A picosecond time-correlated single photon counting (TCSPC) system was used for time-resolved fluorescence and fluorescence anisotropy decay measurements. The system consisted of a self-mode-locked and cavity-dumped femtosecond Ti:sapphire laser pumped by a continuous wave (cw) Nd:YAG laser (Coherent, Verdi). The full width at half-maximum of the instrument response function obtained by a dilute solution of coffee cream was typically 50 ps in our TCSPC system. The fluorescence decays were measured with magic-angle emission polarization, and the number of fluorescence photons per unit time, detected by photomultiplier tube, was always maintained to <1% of the repetition rate of the excitation pulses, to prevent pile-up distortions in the decay profiles. Time-resolved fluorescence anisotropy decays were obtained by changing the detection polarization on the fluorescence path parallel or perpendicular to the polarization of the excitation light. The anisotropy decays then were calculated as follows:

$$r(t) = \frac{I_{VV}(t) - GI_{VH}(t)}{I_{VV}(t) + 2GI_{VH}(t)} \quad (1)$$

where $I_{VV}(t)$ (or $I_{VH}(t)$) is the fluorescence decay when the excitation light is vertically polarized and only the vertically (or horizontally) polarized portion of fluorescence is detected, denoting that the first and second subscripts represent excitation and detection polarization, respectively. The factor G is defined by $I_{VV}(t)/I_{VH}(t)$, which is equal to the ratio of the sensitivities of the detection system for vertically and horizontally polarized light. The G factor of our detection system was 1.08. The fittings for both isotropic and anisotropic decays were performed by a least-squares deconvolution fitting process. The vertical and horizontal components of fluorescence emission were simultaneously fitted to extract the anisotropy decay functions, using the LIFETIME program with an iterative nonlinear least-squares deconvolution procedure that was developed at the University of Pennsylvania.[16]

Transient Absorption and Transient Absorption Anisotropy. The dual-beam femtosecond time-resolved transient absorption spectrometer consisted of a self-mode-locked femtosecond Ti:sapphire oscillator (Coherent, MIRA), a Ti:sapphire regenerative amplifier (Clark MXR model TRA-1000) that was pumped by a Q-switched Nd:YAG laser (Clark MXR model ORC-1000), a pulse stretcher/compressor, an optical parametric amplifier (Clark MXR OPA), and an optical detection system. A femtosecond Ti:sapphire oscillator pumped by a cw Nd:YVO_4 laser (Coherent, Verdi) produces a train of ~80-fs mode-locked pulses with an averaged power of 650 mW at 800 nm. The amplified output beam regenerated by chirped pulse amplification (CPA) had a pulse width of ca. 150 fs and a power of ca. 1 W at a repetition rate of 1 kHz, which was divided into two parts by a 1:1 beam splitter. One part was color-tuned for the pump beam by an optical parametric generation and amplification (OPG-OPA). The resulting laser pulse had a temporal width of ~150 fs in the vis/IR range. The pump beam was focused to a spot diameter of ~1 mm, and the laser fluence was adjusted, using a variable neutral-density filter. The other part was focused onto a flowing water cell to generate a white-light continuum, which was again split into two parts. One part of the white-light continuum was overlapped with the pump beam at the sample to probe the transient, while the other part of the white-light continuum was passed through the sample without overlapping the pump beam. The time delay between pump and probe beams was controlled by making the pump beam travel along a variable optical delay line. The white-light continuum beams after the sample were sent through an appropriate interference filter and then were detected by two photodiodes. The outputs from the two photodiodes at the selected wavelength were processed by a combination of a boxcar averager and a lock-in amplifier,

(16) (a) Wild, U. P.; Holzwarth, A. R.; Good, H. P. *Rev. Sci. Instrum.* **1977**, *48*, 1621. (b) Kim, Y.-R.; Hahn, J.-S.; Hong, H.; Jeong, W.; Song, N. W.; Shin, H.-C.; Kim, D. *Biochim. Biophys. Acta* **1999**, *1429*, 486.

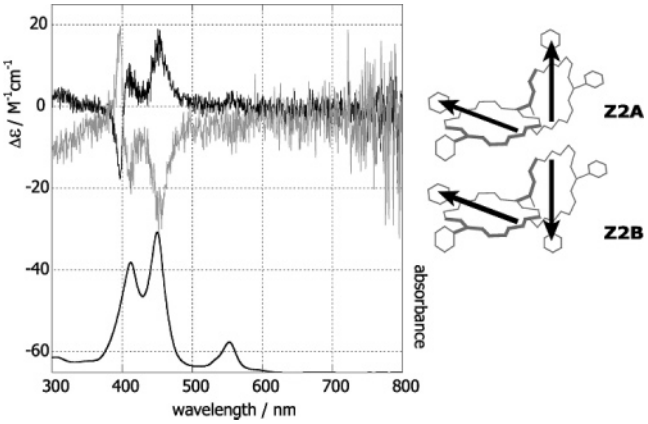

Figure 1. (Bottom) Absorption spectrum of **Z2**. (Top) CD spectra of **Z2** in CH_2Cl_2; the fast eluting isomer **Z2A** (bold line) and the second eluting isomer **Z2B** (thin line).

to calculate the absorption difference at the desired time delay between pump and probe pulses. For the transient absorption anisotropy decay ($r(t)$) measurements, the probe white-light continuum pulse was set to have vertical polarization using a sheet polarizer. The excitation pulse then was changed to have parallel or perpendicular polarization by rotating a half wave plate, with respect to the polarization of the probe pulse. Finally, the transient absorption anisotropy decay was obtained by the following equation,

$$r(t) = \frac{\Delta A_{VV}(t) - \Delta A_{HV}(t)}{\Delta A_{VV}(t) + 2\Delta A_{HV}(t)} \quad (2)$$

where the variable represents amplitude. The fittings for anisotropic decays were performed by a least-squares deconvolution fitting process. The vertical and horizontal components of TA decay were simultaneously fitted to extract the anisotropy decay functions.

Results and Discussion

Synthesis and Characterization. 5,10-Bis(3,5-di-*tert*-butylphenyl)-substituted zinc(II) porphyrin (**Z1**)[5a] was employed as a building block to construct the cyclic arrays. Coupling reaction of **Z1** with $AgPF_6$ in $CHCl_3$ afforded dimer **Z2** (24%), trimer **Z3** (7%), and higher oligomers (Chart 2). Since a free rotation around the *meso*−*meso* bond is strictly prohibited,[17] **Z2** is chiral and **Z3** is diastereoisomeric, which will complicate higher coupling products of **Z2** and **Z3**. To avoid this burdensome situation, **Z2** was optically separated into two enatiomers **Z2A** and **Z2B** through a chiral HPLC column (Supporting Information). Figure 1 shows the absorption and CD spectra of the first and second eluting **Z2** isomers. The CD spectra of the two isomers are weak but perfect mirror images of each other. In the CD spectrum of the fast eluting isomer, the first Cotton effect with positive sense was observed around the low energy Soret band and the second one was observed as a bisignate split Cotton effect with positive sense at the high energy Soret band. The bisignate Cotton effect at the high energy Soret band is arising from coupling of B_x and B_y transition dipole moments by sensing a subtle difference in chiral environment associated with the presence or absence of side *meso*-aryl substituent. Therefore, on the basis of these Cotton effects and empirical

(17) Yoshida, N.; Osuka, A. *Tetrahedron Lett.* **2000**, *41*, 9287.

Chart 2. Porphyrin **Z1** and Its Oligomers (Ar = 3,5-Di-*tert*-butylphenyl)

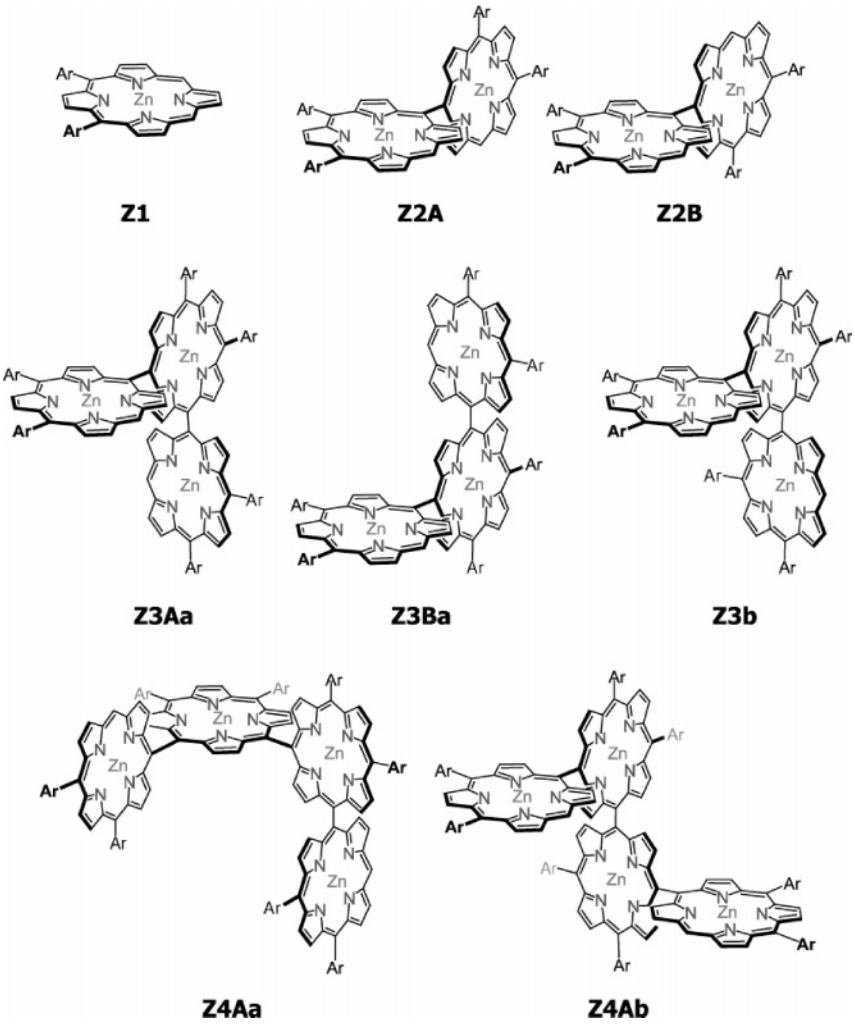

exciton chirality methods and the related studies,[18] the first eluting isomer has been assigned as **Z2A** and the second one as **Z2B**.

Then, the optically pure **Z2A** was coupled to tetraporphyrin **Z4A** (40%), hexaporphyrin **Z6A** (10%), and higher oligomers (ca. 6%). The **Z4A** products were then separated by chromatography over a silica gel column into two diastereoisomers **Z4Aa** and **Z4Ab**. At this stage, **Z4Ab** is expected to be a suitable precursor of cyclic porphyrin arrays, but it is difficult to assign these diasterosiomeric **Z4A** products. Thus, we attempted the silver(I)-promoted coupling of both tetraporphyrins. Upon treatment with $AgPF_6$, a slowly eluting tetramer in $CHCl_3$ (3.3 mM) gave octameric porphyrin ring **CZ8** in 29% yield together with other noncyclic oligomers, while the other tetraporphyrin isomer gave only linear noncyclic oligomers. These results led us to assign the fast and slowly eluting diasteroisomeric tetramers as **Z4Aa** and **Z4Ab**, respectively. Interestingly, under dilute conditions (0.02 mM), the intramolecular cyclization of **Z4Ab** gave tetrameric porphyrin ring **CZ4** preferentially in 74% yield.

(18) (a) Nakanishi, K.; Berova, N. In *Circular Dichroism: Pronciples and Applications*; Nakanish, K., Berova, N., Woody, R. W., Eds.; VCH Publishers Inc.: NewYork, 1994; p 361. (b) Mason, S. F. *Molecular Optical Activity and the Chiral Discriminations*; Cambridge University Press: Cambridge, 1982. (c) Harada, N.; Nakanishi, K. *Acc. Chem. Res.* **1972**, *5*, 257. But the final determination of the stereochemistry will be done through X-ray crystallography.

The triporphyrin fraction **Z3** was separated into two diasteroisomers, an entiomeric pair of **Z3Aa** and **Z3Ba** and *meso*-isomer **Z3b**, by chromatography over a silica gel column. At this step, it is difficult to assign the isomers. As is similar to the case of **Z4Ab**, the *meso*-isomer **Z3b** having two free *meso*-positions on the same side is expected to give a cyclic array. Upon treatment with $AgPF_6$ at 0.1 mM in $CHCl_3$ for 2 h, the slowly eluting triporphyrin gave coupling products, from which hexameric porphyrin ring **CZ6** was isolated in 22% yield as a first eluting fraction. On the other hand, the fast eluting triporphyrin did not give such a porphyrin ring product. On the basis of these experiments, the slowly eluting triporphyrin has been assigned as the *meso*-isomer **Z3b**.

The structures of **CZ4**, **CZ6**, and **CZ8** were characterized by mass spectroscopy and NMR spectroscopy. The peaks observed in electrospray ionization mass (ESI-MS) are *m*/*z* 1493.67 for **CZ4** corresponding to $[M + 2H]^{2+}$, *m*/*z* 1497.00 for **CZ6** corresponding to $[M + 3H]^{3+}$, and *m*/*z* 1996.22 for **CZ8** corresponding to $[M + 3H]^{3+}$, which all support their structures (Supporting Information). The symmetric cyclic structures have been indicated by their very simple ^1H NMR spectra, which all exhibit only a single set of porphyrins (Figure 2). These simple spectra are in sharp contrast to those of noncyclic porphyrin arrays (Supporting Information). Four β-peripheral protons (designated as H^1, H^2, H^3, and H^4 in Figure

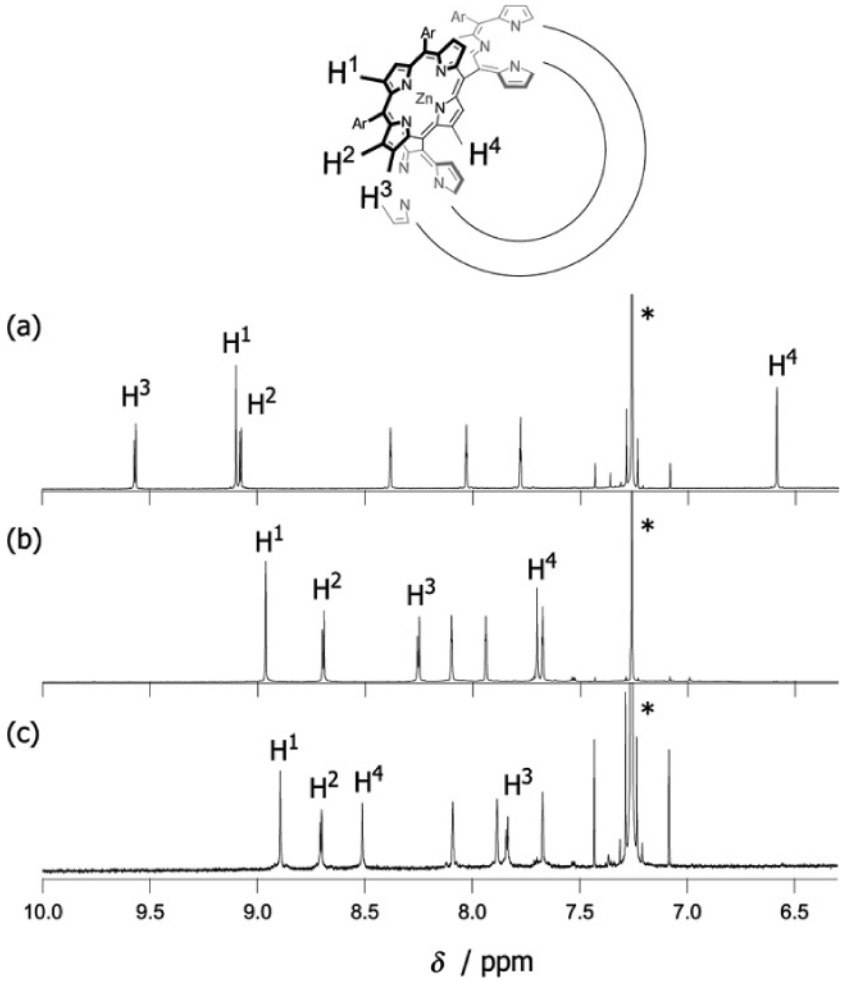

Figure 2. ^{1}H NMR spectra of (a) **CZ4**, (b) **CZ6**, and (c) **CZ8** in $CDCl_3$. The nonlabeled three peaks around 8 ppm were assigned to Ar−H.

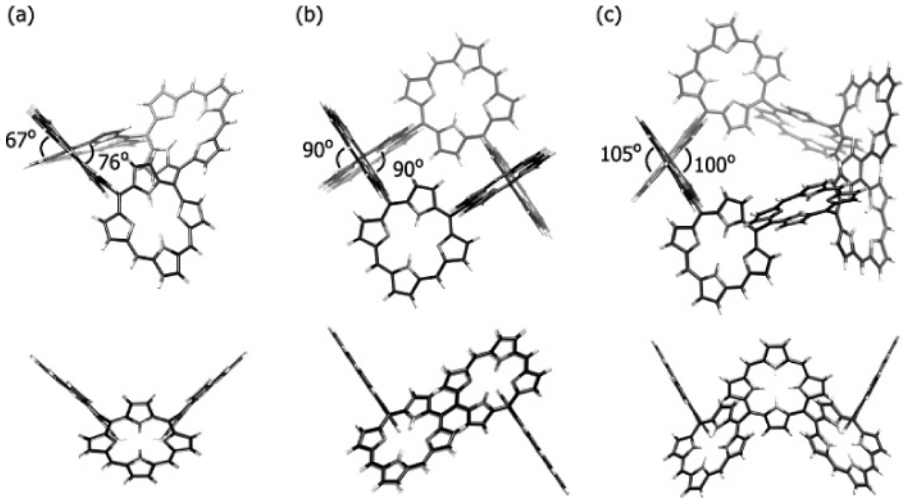

Figure 3. Energy-minimized structures of simplified (a) **CZ4**, (b) **CZ6**, and (c) **CZ8**, in which *meso*-substituents were omitted and zinc atoms were substituted for H_2.

2) are differentiated in these porphyrin rings, and their assignments have been accomplished by comprehensive ROESY measurements and are presented in Figure 2. Of the four β-peripheral protons, the chemical shifts of H^3 and H^4 that are adjacent to the *meso*−*meso* linkage exhibit large changes depending on the molecule; the chemical shift of H^3 is 9.57 ppm in **CZ4**, 8.25 ppm in **CZ6**, and 7.84 ppm in **CZ8**, and that of H^4 is 6.59 ppm in **CZ4**, 7.70 ppm in **CZ6**, and 8.51 ppm in **CZ8**. To explain these observations, theoretical calculations at the B3LYP/6-31G* level were performed to gain respective energy minimized structures (Figure 3). The calculations have revealed that **CZ6** takes a nearly orthogonal conformation with quite planar porphyrins, where 5,15-axes of the neighboring porphyrins are aligned collinear with a 180° angle. In the energy minimized structure of **CZ4**, each porphyrin ring is significantly distorted as suggested by a mean plane deviation of 0.13 Å,

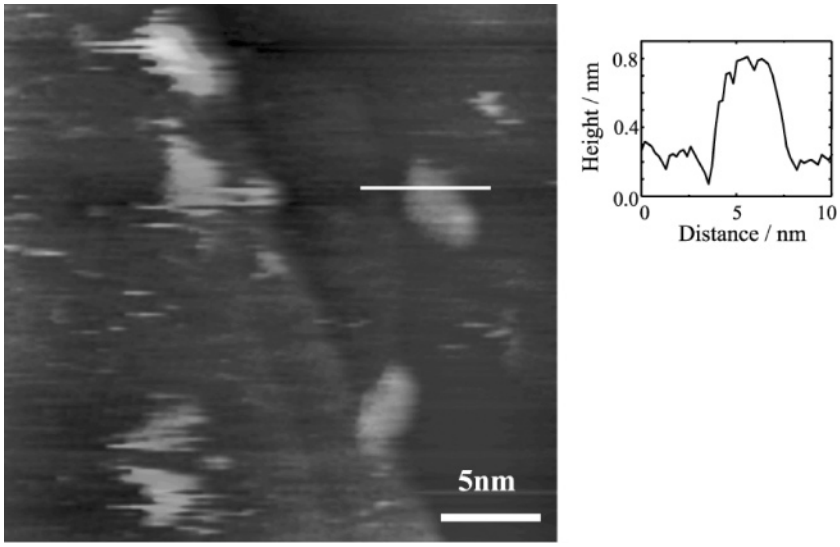

Figure 4. STM image of **CZ8** on Cu(100). (Inset) Height profile along the bar.

Chart 3. Structures of Linear Porphyrin Oligomers $\mathbf{Z_0}n$

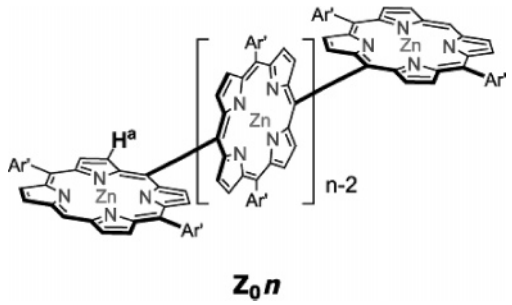

and 5,15-axes of the neighboring porphyrins are bent to 164°. In the calculated structure of **CZ8**, the porphyrin rings are discernibly distorted as suggested by a less mean plane deviation of 0.054 Å and 5,15-axes of the neighboring porphyrins are bent to an angle of 187°. Importantly, the dihedral angles between neighboring porphyrins in the energy minimized structures are 90° in **CZ6**, 76° (inner) and 67° (outer) in **CZ4**, and 100° (inner) and 105° (outer) in **CZ8**. In the exact perpendicular conformation as expected for **CZ6**, the spatial positions of H^3 and H^4 toward the neighboring porphyrin are the same. This situation is similar to the parent *meso*−*meso* linked diporphyrin $\mathbf{Z_0 2}$, in which the H^a proton (designated in Chart 3) appears at 8.12 ppm, being similar to H^3 (8.25 ppm) in **CZ6**. Then, a more high field shifted chemical shift of H^4 can be accounted for in terms of additional shielding effect of the neighboring porphyrin ring. The observed large changes in the chemical shifts of H^3 and H^4 in **CZ4** and **CZ8** can be explained by the calculated structures, since the bending at the *meso*−*meso* linkage causes different environments for H^3 and H^4. In **CZ4**, H^4 is forced to move closer and in a more shielding region and H^3 is shifted remote and in a deshielding region toward the neighboring porphyrin. The trend is reversed and weakened in **CZ8**, reflecting modest bending toward the opposite direction. The similar features have been well demonstrated in a series of strapped *meso*−*meso* linked diporphyrins.[19a]

STM Images of CZ8. Recently we have succeeded in the STM detection of the dodecameric porphyrin ring as a discrete ring.[13] Following the same method, we attempted to take STM images of **CZ8**. A dilute solution of **CZ8** in CH_2Cl_2 was sprayed by using a pulse injection method onto a clean flat Cu(100) surface obtained by cycles of annealing and Ar-ion sputtering.[15] In situ STM measurements were performed at room temperature in a ultrahigh vacuum ($<10^{-10}$ mbar) in a constant height mode. It turned out, however, that the STM detection of **CZ8** was very difficult probably due to weaker adsorption of the molecule on the metal surface. The STM images of **CZ8** taken at a sample bias voltage of 1.5 V and a tunneling current of 52 pA reveal nonlinear but ellipsoid spots with a major axis of ca. 5.3 nm and a minor axis of ca. 3.6 nm (Figure 4), which are overestimated by ca. 1 nm in both axes because of a finite curvature of the STM tip. The size estimated from the STM image is roughly consistent with the calculated structure. An estimated height of the STM images is ca. 5.7 Å, which is rather higher compared with the STM images of other linear and cyclic *meso*−*meso* linked porphyrin arrays.

Excitonic and Electronic Couplings within Cyclic Porphyrin Arrays. The linear *meso*−*meso* linked zinc(II) porphyrin arrays $\mathbf{Z_0}n$ show exciton split Soret ($S_0 \rightarrow S_2$) transition bands due to dipole−dipole exciton couplings between zinc(II) porphyrin units (Figure 5a and Scheme 1).[10] Although two almost degenerate transition dipoles B_x and B_y create one Soret band in a zinc(II) porphyrin monomer, the dipole couplings between adjacent zinc(II) porphyrin units, such as $B_z - B_z$ at opposite, $B_x + B_y$ at orthogonal, and $B_z + B_z$ at parallel, generate three nondegenerate transition dipoles and concomitantly two separate Soret bands in the directly linked zinc(II) diporphyrin ($\mathbf{Z_0 2}$). Low energy Soret ($B_z + B_z$) and Q-bands are continuously red-shifted with an increase in the number of porphyrins ($\mathbf{Z_0 4} < \mathbf{Z_0 6} < \mathbf{Z_0 8}$). In sharp contrast, the porphyrin rings **CZ4**, **CZ6**, and **CZ8** exhibit characteristic broad Soret bands that are centered around 460 nm and are slightly red-shifted in going from **CZ4** to **CZ6** and **CZ8** (Figure 5b and Table 1). These observations can be well explained by their symmetric cyclic structures, in which all the B_x and B_y dipole moments are involved in the exciton coupling (Scheme 1). The symmetric

(19) (a) Yoshida, N.; Ishizuka, T.; Osuka, A.; Jeong, D. H.; Cho, H. S.; Kim, D.; Matsuzaki, Y.; Nogami, A.; Tanaka, K. *Chem.—Eur. J.* **2003**, *9*, 58. (b) Shinmori, H.; Ahn, T. K.; Cho, H. S.; Kim. D.; Yoshida, N.; Osuka, A. *Angew. Chem., Int. Ed.* **2003**, *42*, 2754.

Scheme 1. Exciton Coupling in Monomer, *meso*−*meso* Linked Dimer, and Cyclic Hexamer **CZ6**

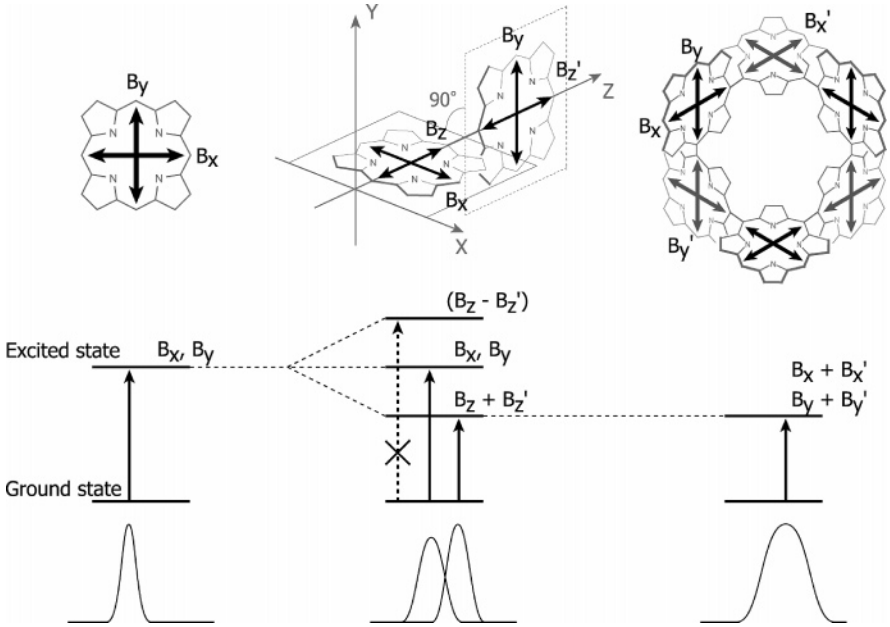

ring structures lead to the repeating same exciton coupling, which causes a single Soret band. The broad and structureless Soret bands indicate that there are some heterogeneities in dipole−dipole couplings between the porphyrin units presumably because of conformational flexibilities (Figure 3). On the other hand, the Q absorption ($S_0 \rightarrow S_1$) tail reveals red-shifts in going from **CZ6** to **CZ8** and **CZ4**. An interesting feature is a sharp shoulder absorption band at 409 nm that is observed only for **CZ4**.

The fluorescence spectra of the linear (**$Z_0$3**, **$Z_0$4**, **$Z_0$6**, and **$Z_0$8**) and cyclic arrays (**CZ4**, **CZ6**, and **CZ8**) are compared in Figure 6. The linear porphyrin arrays show fluorescence ($S_1 \rightarrow S_0$)

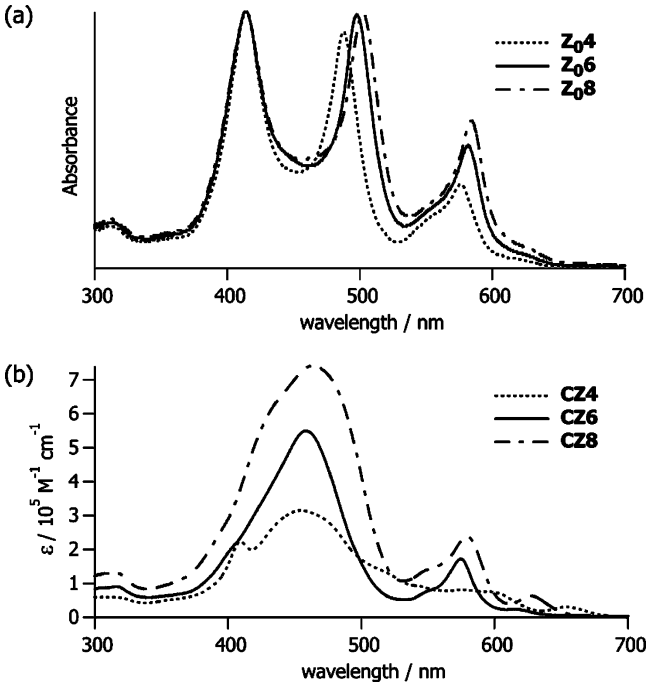

Figure 5. Absorption spectra of porphyrin arrays in THF; (a) 5,15-*meso*−*meso* linked linear oligomers **$Z_0$4**, **$Z_0$6**, and **$Z_0$8** (absorbances are normalized around 413 nm) and (b) **CZ4**, **CZ6**, and **CZ8**.

Table 1. Absorption and Fluorescence Data of **CZ4**, **CZ6**, and **CZ8** in THF

	absorption[a] (nm)				fluorescence[b] (nm)		
sample	soret (high)	soret (low)	*Q*(1,0)	*Q*(0,0)	*Q*(0,0)	Q(0,1)	Φ_f[c]
CZ4	409 (220 000)	454 (310 000)	594 (76 000)	654 (31 000)	674	727	0.071
CZ6		458 (550 000)	575 (170 000)	615 (22 000)	631	675	0.031
CZ8		464 (740 000)	580 (240 000)	628 (64 000)	646	685	0.040

[a] Molar extinction coefficient (M^{-1} cm^{-1}) is presented in parentheses. [b] $\lambda_{ex} = 455$ nm. [c] Quantum yield was determined with reference to the value ($\Phi_f = 0.033$) of zinc(II) tetraphenylporphyrin in benzene.

spectra with two bands at 640 and 667 nm, and the intensity of the higher energy band increases with an increase in the number of porphyrins (**$Z_0$3** < **$Z_0$4** < **$Z_0$6** < **$Z_0$8**). On the other hand, the fluorescence spectra of the cyclic arrays look more diverse in shape, band position, and intensity. The fluorescence of the cyclic arrays reveal red-shifts in the order **CZ6** < **CZ8** < **CZ4**, in line with their Q-band tail positions, and the fluorescence intensity increases in the order **CZ6** < **CZ8** < **CZ4**. The band positions and structures in the absorption and fluorescence spectra suggest unique excitonic and electronic communications between the constituent porphyrin units.

According to our previous reports, the electronic couplings between porphyrin units can be well related to the dihedral angle between porphyrin units.[19] The strapped zinc(II) diporphyrin, where the strapping carbon chain controls a dihedral angle between two zinc(II) porphyrin units, shows that the smaller dihedral angle between porphyrin units gives rise to the stronger electronic coupling and concomitantly red-shifts in the Q absorption and fluorescence spectra.[19b] As a consequence, the Q absorption and fluorescence spectra indicate the electronic coupling strength increases in the order **CZ6** < **CZ8** < **CZ4** in accordance with the dihedral angle estimated from the above ^{1}H NMR data and geometry optimization. On the basis of the energy minimized structures in Figure 3, we will use values of 72° for **CZ4**, 90° for **CZ6**, and 77° for **CZ8** as the effective

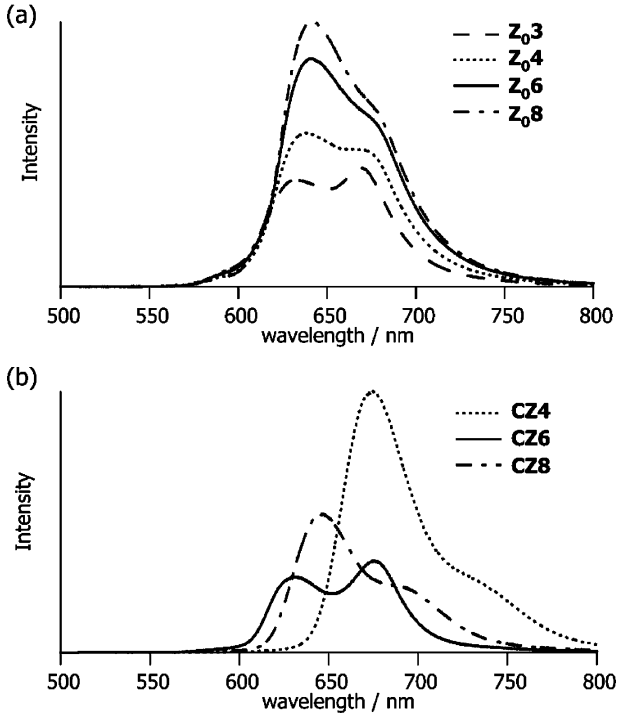

Figure 6. Fluorescence spectra of **CZ4**, **CZ6**, and **CZ8** taken for excitation at 455 nm in THF.

dihedral angle between neighboring porphyrins in the following discussion. It is interesting to note that the fluorescence of **CZ6** is quite similar to that of $\mathbf{Z_0 3}$, in line with its estimated 90° dihedral angle. The small absorption shoulder at 409 nm in **CZ4** may be understood in terms of H-type dipole−dipole coupling only occurring in zinc(II) porphyrin units with a small dihedral angle, which gives rise to a more blue-shifted Soret band (409 nm) than the high energy Soret band (417 nm)[20] of $\mathbf{Z_0 2}$. Finally, we need to look into the exciton and electronic couplings from a viewpoint of energy transfer. Because the cyclic arrays have strong excitonic and electronic couplings between porphyrin units, the coherent and/or incoherent energy hopping processes are easily expected.

Fluorescence Lifetimes and Rotational Diffusion Motions of Cyclic Porphyrin Arrays. The time-resolved fluorescence decay profiles of the cyclic arrays are displayed in Figure 7, and their fitted parameters are summarized in Table 2. The fluorescence decays do not show any emission wavelength dependence, implying single-exponential relaxations from the lowest singlet S_1 states of porphyrins. The fitted S_1 state lifetimes slightly depend on the size of the cyclic array, decreasing in the order **CZ4** < **CZ8** < **CZ6**, which are consistent with their steady-state fluorescence quantum yields (Tables 1 and 2). An interesting feature is that the S_1 state lifetime decreases in the same order of the blue-shifts in the Q absorption and fluorescence spectra. According to the previous work on linear zinc(II) porphyrin arrays, the S_1 state lifetimes gradually decrease as the number of porphyrin units increases as a result of the enhanced conformational heterogeneities in the longer arrays.[12b,21] The S_1 state lifetime of 1.84 ns in **CZ4** is distinctly longer than 0.92 ns in linear zinc(II) porphyrin tetramer $\mathbf{Z_0 4}$.[21] In addition,

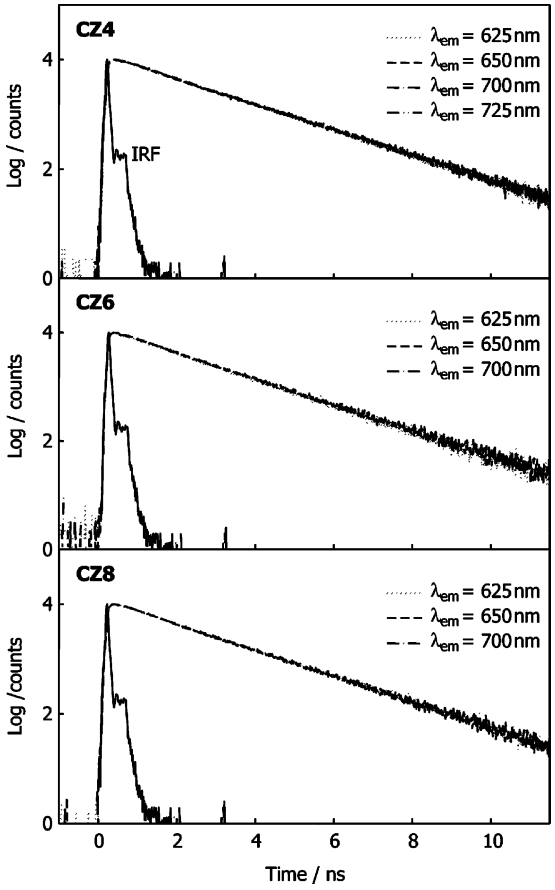

Figure 7. Time-resolved fluorescence decay profiles of **CZ4**, **CZ6**, and **CZ8** measured by using the excitation wavelength 420 nm in THF.

Table 2. Fitted Fluorescence Lifetimes and Anisotropy Decay Parameters of **CZ4**, **CZ6**, and **CZ8** in THF[e]

	fitted fluorescence lifetime[a]	anisotropy decay parameters[c]	
sample	τ[b] (ns)	r_0[d]	Φ[d] (ns)
CZ4	1.84 ± 0.02 (100%)	0.036 ± 0.007	0.94 ± 0.31
CZ6	1.76 ± 0.04 (100%)	0.009 ± 0.005	1.50 ± 0.50
CZ8	1.80 ± 0.02 (100%)	−0.019 ± 0.005	2.88 ± 0.75

[a] The fluorescence lifetimes of the samples were obtained by averaging the fitted single fluorescence lifetimes at several emission wavelengths. [b] Using the relation $I(t) = A \exp(-t/\tau)$, where $I(t)$ is the time-dependent fluorescence intensity, A, the amplitude (noted in parentheses as the percentage), and τ, the fitted fluorescence lifetime; the χ^2 values of the fittings were maintained as ∼1.0−1.3. [c] The fluorescence anisotropy decays were monitored at λ_{em} = 670 nm. [d] Using the relation $r(t) = r_0 \exp(-t/\Phi)$, where $r(t)$ is the time-dependent fluorescence anisotropy $[r(t) = (I_{||}(t) - GI_{\perp}(t))/(I_{||}(t) + 2G\,I_{\perp}(t))$, r_0, the initial anisotropy value, and Φ, the fitted anisotropy decay time. [e] The excitation wavelength, 420 nm, was applied to all experiments.

the dependence of the S_1 state lifetime on the ring size is negligible in comparison with the linear zinc(II) porphyrin array $\mathbf{Z_0}\boldsymbol{n}$.[12b,21] These results indicate that the conformational motions or the nonradiative relaxation processes of **CZ4**, **CZ6**, and **CZ8** are considerably restricted in the ring structures. It is to be noted that the increased S_1 state lifetime has an apparent advantage in the excitation energy transfer process.

The fluorescence anisotropy decay profiles of the cyclic arrays are presented in Figure 8, where the excitation of the high energy Soret band (λ_{ex} = 420 nm) was employed. The fitted decay parameters are tabulated in Table 2. The anisotropy decay times do not reflect the energy migration processes within **CZ4**, **CZ6**, and **CZ8**, because their time scales (∼1.0−3.0 ns) are consider-

(20) Hwang, I.-W.; Cho, H. S.; Jeong, D. H.; Kim, D.; Tsuda, A.; Nakamura, T.; Osuka, A. *J. Phys. Chem. B* **2003**, *107*, 9977.
(21) Cho, S. H.; Song, N. W.; Kim, Y. H.; Jeoung, S. C.; Hahn, S.; Kim, D.; Kim, S. K.; Yoshida, N.; Osuka, A. *J. Phys. Chem. A* **2000**, *104*, 3287.

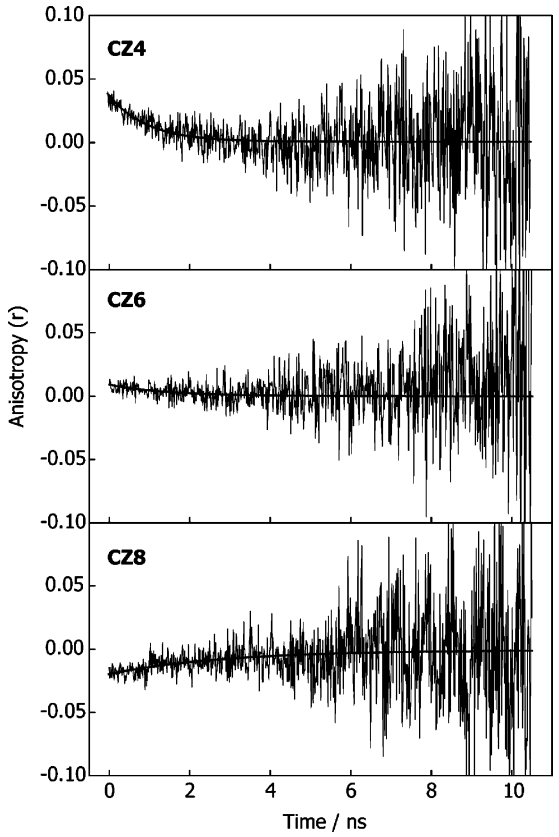

Figure 8. Time-resolved fluorescence anisotropy decay profiles of **CZ4**, **CZ6**, and **CZ8**. The polarized fluorescence decays ($I_{VV}(t)$ and $I_{VH}(t)$) are measured at the emission wavelength 670 nm, and then the anisotropy decays $r(t)$ are calculated by eq 1. The decays are obtained using the excitation wavelength 420 nm in THF.

ably slow in view of the close proximity intermolecular geometries. Instead, the decay times (Φ) are well associated with the molecular rotational diffusion times in solution, illustrating slower motions in larger cyclic arrays (Table 2). In addition, the different initial r_0 values plausibly result from the different angles between absorption and emission dipoles as well as the efficient energy transfer processes along the cyclic arrays.

EEH Processes in Cyclic Porphyrin Arrays. To investigate the EEH process along the cyclic array, femtosecond transient absorption (TA) and transient absorption anisotropy (TAA) decays are simultaneously measured (Figures 9 and 10), where the *Q*-band excitation ($\lambda_{pump} = 583$ nm) is employed to avoid an involvement of S_2-S_1 relaxation in the porphyrin. As displayed in Figures 9 and 10, the cyclic arrays reveal intensity dependent TA decays along with TAA rises in the time scale of hundreds of femtoseconds, indicating exciton−exciton annihilation and depolarization channels contributed by EEH processes. The TA decays are deconvoluted with two decay components (τ_1 and τ_2), where the slow τ_2 components are fixed as the S_1 state lifetimes as revealed by the fluorescence decay measurements (Table 3). The TAA rises are also deconvoluted with one rising component, of which the fitted parameters are inserted in Figure 10.

The TA decays depend on the pump power as well as the size of the porphyrin ring (Figure 9 and Table 3). As the pump power is increased, the relative contribution of the fast τ_1 component is enhanced as compared with the long-lived one. In addition, the τ_1 values systematically increase from 73 to

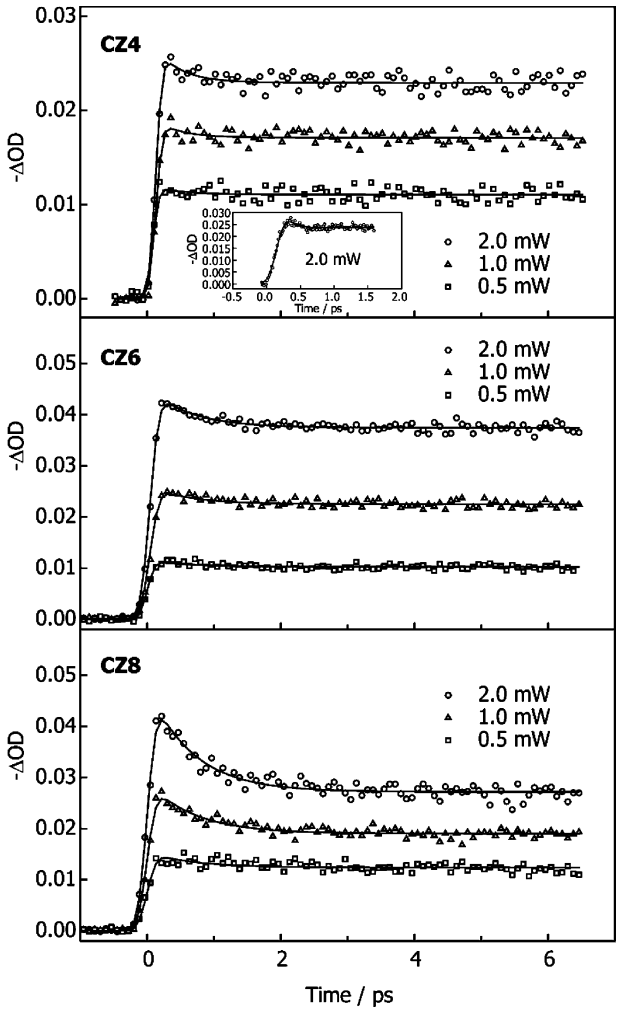

Figure 9. Transient absorption decay profiles of **CZ4**, **CZ6**, and **CZ8** that include pump-power dependences in THF, where the pump and probe wavelengths are 583 and 460 nm, i.e., the Q-band pump and bleaching recovery probe. The decays are measured with magic angle polarization between pump and probe beams.

560 fs and 680 fs in going from **CZ4** to **CZ6** and **CZ8**, i.e., as the size of the cyclic array increases. The pump-power dependence on the TA decay is indicative of the exciton−exciton annihilation process, because intense excitation or high density of photons generates two or more excitons in one cyclic array, and then the recombination process between them creates a fast deactivation channel.[22,23] According to the previous description on the natural light-harvesting antennae such as LH1 and LH2, the exciton−exciton annihilation process is conceived as a Förster-type incoherent EEH process from the excited donor to the proximal excited acceptor resulting in a doubly excited acceptor state; the latter quickly relaxes to the singly excited state.[22,23] Therefore, the exciton−exciton annihilation process should be a direct evidence of the Förster-type incoherent EEH process within the cyclic array. Figure 9 and Table 3 also indicate that the exciton−exciton annihilation process is due to

(22) Bradforth, S. E.; Jimenez, R.; van Mourik, F.; van Grondelle, R.; Fleming, G. R. *J. Phys. Chem.* **1995**, *99*, 16179.
(23) (a) Trinkunas, G.; Herek, J. L.; Polívka, T.; Sundström, V.; Pullerits, T. *Phys. Rev. Lett.* **2001**, *86*, 4167. (b) Trinkunas, G. *J. Lumin.* **2003**, *102*, 532. (c) Brüggemann, B.; May, V. *J. Chem. Phys.* **2004**, *120*, 2325. (d) Müller, M. G.; Hucke, M.; Reus, M.; Holzwarth, A. R. *J. Phys. Chem.* **1996**, *100*, 9537. (e) Brüggemann, B.; Herek, J. L.; Sundström, V.; Pullerits, T.; May, V. *J. Phys. Chem. B* **2001**, *105*, 11391.

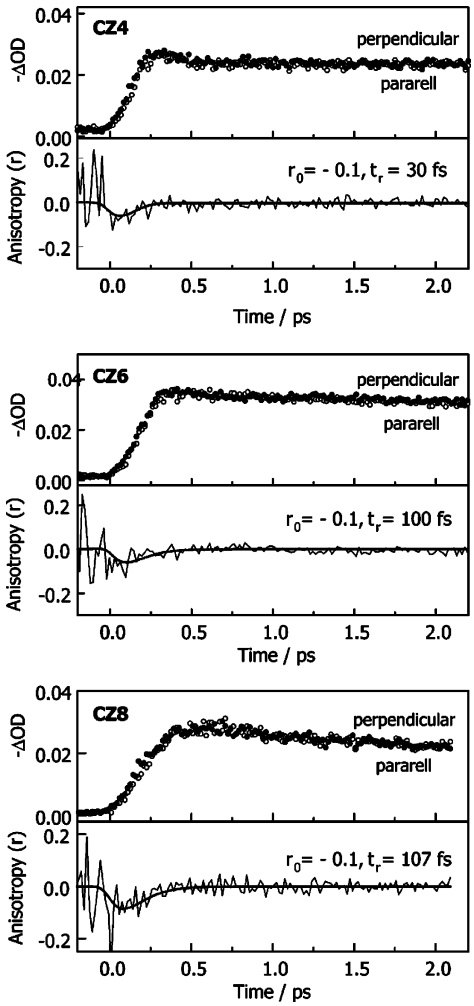

Figure 10. Transient absorption anisotropy decay profiles of **CZ4**, **CZ6**, and **CZ8** in THF, where the polarized transient absorption decays for parallel and perpendicular orientations between pump and probe beams are also included. Insets show the deconvolution fitted decay parameters with a train of 150-fs pump pulses. The pump and probe wavelengths are 583 and 460 nm, which are the Q-band pump and bleaching recovery probe.

Table 3. Transient Absorption Decay Parameters for **CZ4**, **CZ6**, and **CZ8** Depending on Pump Power[a]

pump power (mW)	fitted decay times[b] (ps) τ_1	τ_2
	CZ4	
2.0	0.073 (14%)	1840 (86%)
1.0	0.073 (9%)	1840 (91%)
0.5	0.073 (8%)	1840 (92%)
	CZ6	
2.0	0.56 (17%)	1760 (83%)
1.0	0.56 (13%)	1760 (87%)
0.5	0.56 (11%)	1760 (89%)
	CZ8	
2.0	0.66 (44%)	1800 (56%)
1.0	0.70 (35%)	1800 (65%)
0.5	0.68 (19%)	1800 (81%)

[a] The pump and probe wavelengths are 583 and 460 nm, respectively. [b] Using the relation $-\Delta OD(t) = A_1 \exp(-t/\tau_1) + A_2 \exp(-t/\tau_2)$, where $\Delta OD(t)$ is the transient absorption intensity, A, the amplitude (noted in parentheses as the normalized percentage, i.e., $[A_i/(A_1 + A_2)] \times 100$), and τ, the fitted decay time. The solvent used was consistently THF.

the migration limited exciton−exciton recombination process along the cyclic array, because this process becomes slow as the size of the traveling ring increases. In addition, it is interesting to note that the exciton migration time of 680 fs in **CZ8** is even faster than ~1 ps[22] in LH2.

The TAA measurement is also a helpful tool to investigate the excitation energy migration process along the cyclic array, because the EEH process even between the same molecular units aligned in different direction creates a depolarization channel. Figure 10 shows the TAA rises arising from the fast energy migration processes along the cyclic arrays. The TAA rise times systematically increase from 30 to 100 fs and 107 fs in going from **CZ4** to **CZ6** and **CZ8**, indicating that the anisotropy rise is also sensitive to the traveling ring size. In a multichromophoric system, neither exciton−exciton annihilation nor anisotropy depolarization time does directly represent the EEH time, because they do not occur between single donor and acceptor unit. The EEH time among the constituent chromophores can be theoretically evaluated by modeling the hopping process and the simultaneous observation of these two observables.[22,23]

The description of the exciton−exciton annihilation and anisotropy depolarization has been well developed for the natural light-harvesting systems such as LH1 and LH2 that have wheel arrangements with constant interchromophore interaction.[22,23] In these complexes, an explicit Förster-type incoherent EEH model has been described assuming a migration-limited character of the exciton−exciton annihilation process and random walk formalism of the anisotropy decay. In this context, the experimentally determined depolarization and exciton−exciton annihilation times are connected with the EEH time by the following equations

$$\tau_{\text{depolarization}} = \frac{\tau_{\text{hopping}}}{4(1 - \cos^2(2\pi/N))} = \frac{\tau_{\text{hopping}}}{4(1 - \cos^2 \alpha)} \quad (3)$$

$$\tau_{\text{annihilation}} = \frac{N^2 - 1}{24}\tau_{\text{hopping}} \quad (4)$$

where N is the number of hopping sites, α, the angle between the adjacent transition dipoles, $\tau_{\text{annihilation}}$, the slowest exciton−exciton annihilation time, and τ_{hopping}, the inverse of the nearest neighbor energy hopping rate. Equation 3 is understood by considering that the depolarization is complete when the transition dipole migrates through 90° and by considering how many hops are required for this rotation to be accomplished. On the other hand, eq 4 assumes that the exciton−exciton annihilation reflects the migration limited exciton−exciton recombination along the cyclic array and how many hops are required for this recombination to be accomplished.

Now, we model the EEH process within the cyclic array and simultaneously use the two different observables, exciton−exciton annihilation and anisotropy decay times, to estimate the EEH time between the hopping sites. Concerning the number of hopping sites, it is conceived as $N = 4$, $N = 6$, and $N = 8$ for **CZ4**, **CZ6**, and **CZ8**, respectively. Although the exciton coherence via two porphyrin units rather than one porphyrin unit is rationalized in the cyclic array, in view of cyclic geometry and exciton coherence length of 4−5 porphyrin units[12] in the Q-state of the directly linked linear array $\mathbf{Z_0}\boldsymbol{n}$, the numbers of excitation energy hopping sites for the cyclic arrays are $N = 4$, $N = 6$, and $N = 8$, as a result of the bidirectional coupling with the nearest neighboring porphyrins in the two-dimensional space

Scheme 2. Excitation Energy Hopping Rates in **CZ4**, **CZ6**, and **CZ8**

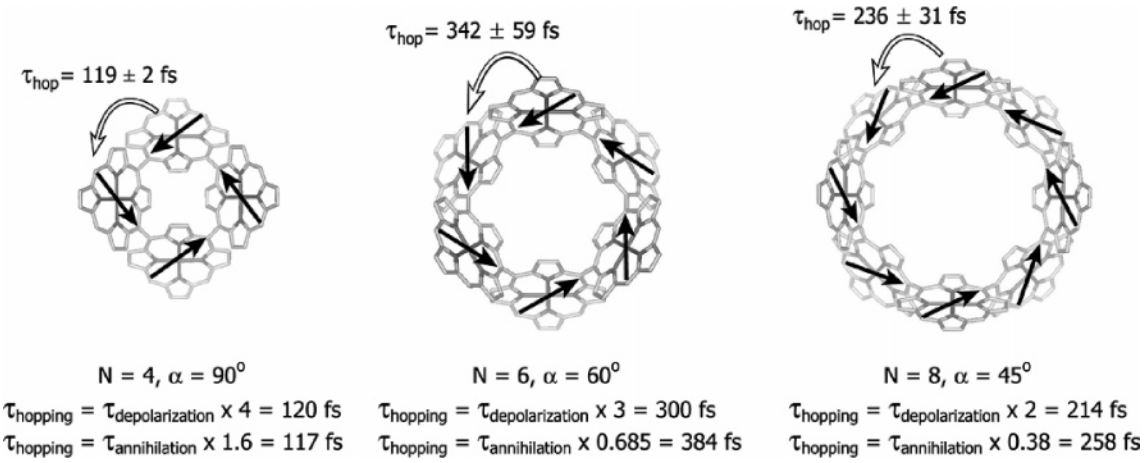

of the cyclic arrays (Scheme 1). To describe the random walk of the anisotropy decay, the orientations of the molecular transition dipole moments should be considered. As shown in Scheme 2, the transition dipoles that are attributable to the change in anisotropy are arranged in the two-dimensional *xy*-plane, where the anisotropy decay profile reflects the EEH between the transition dipoles. This modeling indicates that the EEH process within the cyclic array can be well described by eqs 3 and 4, which are applicable to a well-defined cyclic molecular array. Introducing $\alpha = 90°$ and $N = 4$ to eqs 3 and 4, the relations $\tau_{hopping} = 4 \times \tau_{depolarization}$ and $\tau_{hopping} = 1.6 \times \tau_{annihilation}$ are obtained for **CZ4**. Similarly, introducing $\alpha = 60°$ and $N = 6$, the relations $\tau_{hopping} = 3 \times \tau_{depolarization}$ and $\tau_{hopping} = 0.685 \times \tau_{annihilation}$ are obtained for **CZ6**. Finally, introducing $\alpha = 45°$ and $N = 8$, the relations $\tau_{hopping} = 2 \times \tau_{depolarization}$ and $\tau_{hopping} = 0.38 \times \tau_{annihilation}$ are obtained for **CZ8**. Consequently, the EEH time constants are calculated to be 120, 300, and 214 fs in **CZ4**, **CZ6**, and **CZ8**, respectively, using the anisotropy rise times of $\tau_r = 30$, 100, and 107 fs given in Figure 10. In a different approach, the EEH time constants are estimated to be 117, 384, and 258 fs using the annihilation times $\tau_1 = 73$, 560, and 680 fs given in Table 3. It is noteworthy that the two different experimental observables, exciton−exciton annihilation and anisotropy depolarization, result in the similar EEH times between zinc(II) porphyrin units, which are 119 ± 2 fs in **CZ4**, 342 ± 59 fs in **CZ6**, and 236 ± 31 fs in **CZ8** (Scheme 2). This coincidence implies that the EEH processes within the cyclic arrays are well described by the Förster-type incoherent energy hopping model because of their well-defined dipole orientations. Finally, the observed EEH times (119 ± 2 fs in **CZ4**, 342 ± 59 fs in **CZ6**, and 236 ± 31 fs in **CZ8**) can be well associated with the red-shifts in the Q absorption and fluorescence spectra, demonstrating that the increased electronic interactions accelerate the EEH processes between zinc(II) porphyrin units. We attribute this trend primarily to the decreased dihedral angle between the neighboring porphyrins in the order **CZ6** > **CZ8** > **CZ4**. Finally, it is interesting to note that the EEH times, i.e., 119 ± 2 fs in **CZ4** and 236 ± 31 fs in **CZ8**, are faster than ~270 fs[23b] in LH2, because of the proximity and stronger electronic couplings in the cyclic porphyrin arrays.

In summary, the directly linked porphyrin rings **CZ4**, **CZ6**, and **CZ8** were synthesized in a stepwise manner from 5,10-diaryl zinc(II) porphyrin **Z1**. These porphyrin ring molecules have been shown to serve as a platform to enable very efficient EEH processes along the ring circuit with rates that rival those of natural cyclic photosynthetic antenna. Future work will focus on incorporation of these functional units into more elaborate model systems and exploration of larger directly linked porphyrin arrays.

Acknowledgment. The work at Kyoto was partly supported by Grant-in-Aid for Scientific Research on Priority Area (No. 16033231, Reaction Control of Dynamic Complexes) from the Ministry of Education, Culture, Sports, Science and Technology, Japan and 21st Century COE on Kyoto University Alliance for Chemistry. The work at Yonsei was supported by the National Creative Research Initiatives Program of the Ministry of Science and Technology of Korea.

Supporting Information Available: Experimental section, ^{1}H NMR spectra, absorption and fluorescence spectra, optical resolution of racemic **Z2**, and GPC-HPLC analysis. This material is available free of charge via the Internet at http://pubs.acs.org.

JA045254P